Accessing thermal conductivity of complex compounds by machine learning interatomic potentials

Pavel Korotaev,[1,2,*] Ivan Novoselov,[1,2] Aleksey Yanilkin,[1,2] and Alexander Shapeev[3]
[1]*Dukhov Research Institute for Automatics, Sushchevskaya 22, Moscow 127055, Russia*
[2]*Moscow Institute of Physics and Technology, Institutskiy Pereulok 9, Dolgoprudny, Moscow Region 141700, Russia*
[3]*Skolkovo Institute of Science and Technology, Skolkovo Innovation Center 3, Moscow 143026, Russia*

(Received 23 July 2019; revised manuscript received 11 September 2019; published 22 October 2019)

While lattice thermal conductivity is an important parameter for many technological applications, its calculation is a time-consuming task, especially for compounds with a complex crystal structure. In this paper, we solve this problem using machine learning interatomic potentials. These potentials trained on the density functional theory results and provide an accurate description of lattice dynamics. Additionally, active learning was applied to significantly reduce the number of expensive quantum-mechanical calculations required for training and increases reliability of the potential. The $CoSb_3$ skutterudite was considered as an example, and the solution of the Boltzmann transport equation for phonons was compared with the Green-Kubo method. We demonstrated that accurate and reliable potentials can be obtained by performing just a few hundred quantum-mechanical calculations. The potentials reproduce not only the vibrational spectrum, but also the lattice thermal conductivity, as calculated by various methods.

DOI: 10.1103/PhysRevB.100.144308

I. INTRODUCTION

Accurate description of lattice dynamics and large time or length scales of a considered phenomenon are both required in many practically important tasks of atomistic modeling. The example is lattice thermal conductivity (LTC) calculations. LTC describes heat transport through a crystalline lattice, which is of prime importance for thermoelectic conversion efficiency, heat insulation, etc.

LTC is usually described in two ways. The first one is the framework of the Boltzmann transport equation for phonons (PBTE) [1–3]. The second one is molecular dynamics (MD) simulation-based methods [4]: the Green-Cubo (GK) method and the direct method.

While the solution of the PBTE allows one to correctly describe the LTC in many cases [5,6], there are two issues limiting its application. Firstly, only three-phonon processes are considered in the scattering, due to high computational cost. Although this is sufficient in many cases, high-order processes may play an impotant role in the heat transfer at high temperatures [7]. Secondly, the method scales poorly for large systems, as $(N_{\text{at}}^4 N_q^2)$ [8], where N_{at} is the number of atoms in the cell, and N_q is the number of points in the reciprocal space grid. This limitation is crucial if the considered system has a complex crystal structure with about 100 atoms in the unit cell. Such systems often have low thermal conductivities, which is important for practical applications.

It is possible to overcome these issues by using methods based on classical MD modeling. They have no restrictions on the order of anharmonic terms and scale better with the system size. The price, however, is the need for a careful convergence analysis [8,9]. But the biggest issue of the method is the interatomic potential. The potential must be accurate in order to reproduce phonon scattering, and reliable in order to allow long-time simulations of large systems.

Similar problems arise for the free energy calculations. The most accurate and approximation-free methods are the analysis of the velocity autocorrelation function and the thermodynamic integration [10,11]. Simulations on large systems and long-time scales are required for such methods. Therefore, the routine *ab initio* molecular dynamics (AIMD) simulations are unfeasible.

Machine learning potentials have recently been proposed as a promising tool to combine quantum-mechanical accuracy with the computational efficiency of classical potentials [12,13]. It is a common and often an easy-to-pass test for machine learning potentials to reproduce force constants or phonon dispersion curves. From these tests it is not clear whether machine learning potentials could accurately describe anharmonicity, which is a small effect compared to harmonic vibrations at small temperatures. Only a few examples of such studies exist in the literature [14–17].

An attractive feature of some of the machine learning potentials is the ability to use uncertainty estimation to generate potentials on-the-fly. The main advantage of using active learning is that potentials that reliably predict energies and forces are constructed automatically while performing lattice dynamics, or another atomistic simulation, rather than manually parametrized through many cycles of trial and error. In this work we will use the D-optimality-based active learning algorithm [18,19]. Other existing approaches rely on query by committee [20–22] and Bayesian predictive variance [23]. A related recently proposed approach [24] is to select a training set using a distance metric alone.

In this work, we develop an algorithm for simulation of LTC by automatically training a machine learning potential in the moment tensor potential (MTP) form [18,19,25]

*korotaev@vniia.ru

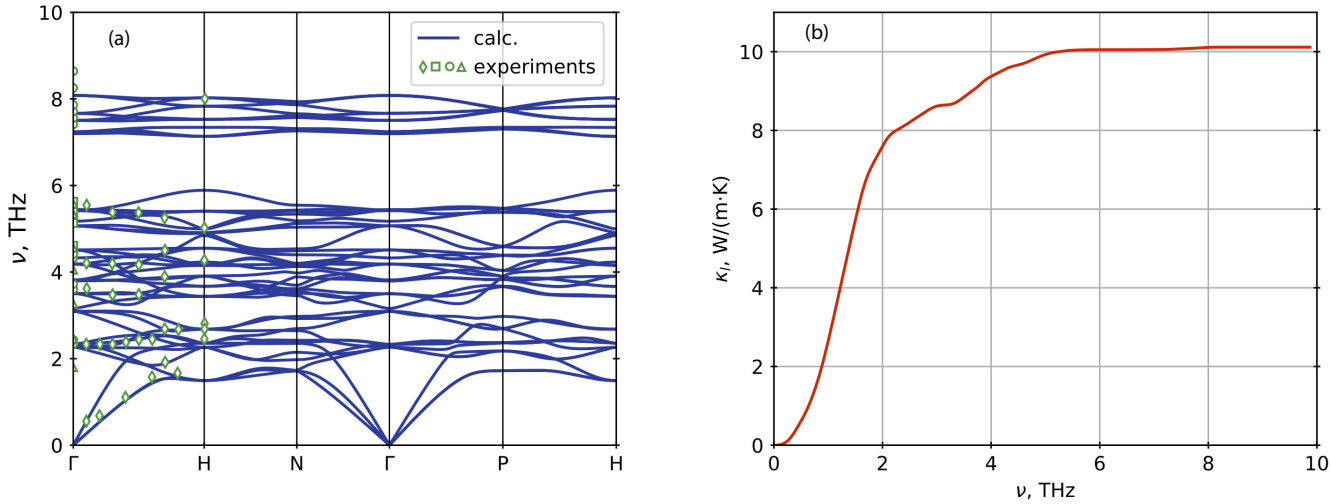

FIG. 1. (a) Calculated phonon dispersion (solid line) and experimental values: (○) [38], (□) [39], (△) [40], and (◇) [41]. (b) The cumulative dependence of LTC on the phonon frequency at 300 K.

on-the-fly. The proposed algorithm is benchmarked on the problem of computing LTC for the $CoSb_3$ skutterudite. Anharmonic lattice vibrations is the main mechanism responsible for the finite LTC. Therefore this is a sensitive test of the accuracy of the potentials.

$CoSb_3$-based materials are of great importance for thermoelectric applications. It is expected that it can replace traditional toxic tellurium-based materials for the middle-temperature region [26,27]. The feature of skutterudites is the possibility to significantly reduce the LTC due to filling or compensation [28–32], without worsening the electronic transport properties.

Here we consider unfilled $CoSb_3$ for the following reasons. Firstly, as will be clear from the presented results, our method deals with the systems with more than 100 atoms in the unit cell. Therefore the extension to the filled case will be straightforward. Secondly, unfilled $CoSb_3$ contains 16 atoms in the unit cell. Therefore, the LTC calculated by the Green-Kubo method can be directly compared with the result of PBTE based on density functional theory (DFT) data, which provides additional validation of the potential.

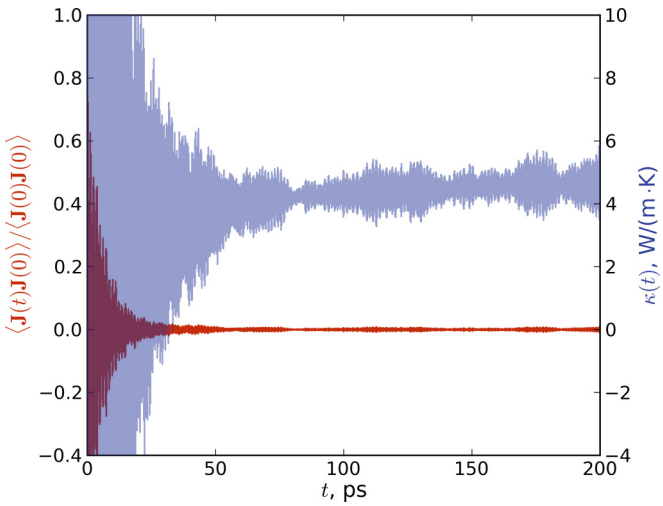

FIG. 2. The normalized heat flux autocorrelation function (red) and the corresponding thermal conductivity (blue) at 500 K.

This paper is orginized as follows. The details of the calculations are discussed in Sec. II. The LTC was calculated using the PBTE, based either on the results of AIMD and classical MD with machine learning potentials. Details are contained in Secs. II A and II B. The same potentials were used in the Green-Kubo method (Sec. II C). The details of training and validation of the potentials are presented in Sec. III. Section IV is devoted to the comparison and discussion of the results. The concluding remarks are given in Sec. V.

II. DETAILS OF CALCULATIONS

A. *Ab initio* molecular dynamics

As the first step, AIMD trajectories were obtained, as described in the previous work on skutterudites [33]. The projector augmented wave [34] VASP [35] code (version 5.4.1) was used for the calculations, with the exchange-correlation functional in the form of Perdew-Burke-Ernzerhof [36]. The $3d^7 4s^2$ Co electrons and $5s^2 5p^3$ Sb electrons were considered as the valence ones. All calculations were performed on $2 \times 2 \times 2$ $Co_{32}Sb_{96}$ supercells containing 128 atoms. The *NVT* thermostat at the temperatures of 300, 500, and 700 K was used. The time step was chosen as 2 fs, and the total simulation time was 6–10 ps. For an accurate calculation of the forces, the cutoff energy of 450 eV and a $2 \times 2 \times 2$ Γ-centered grid of k points (eight points in the irreducible Brillouin zone) were used. The experimental lattice constant was utilized for each temperature, corresponding to the thermal expansion coefficient $\alpha = 9.9 \times 10^{-6}$ 1/K [37]: $a = 4.5182$ Å, 4.5272 Å, and 4.5361 Å for 300, 500, and 700 K, respectively.

B. Lattice thermal conductivity via the Boltzmann transport equation for phonons

At this step, *ab initio* and classical MD trajectories were used to calculate the effective force constants of the

second and third orders. Classical trajectories with MTPs (see Sec. III A) were obtained via the LAMMPS [42] package for the $2 \times 2 \times 2$ cells (as in the AIMD simulations). The systems were equilibrated for 5 ps. Then a 20 ps simulation in the *NVE* ensemble was conducted, during which the statistics was generated.

The force constants were determined by constructing a temperature-dependent effective potential [43,44]. Effective second- and third-order potentials were obtained by matching the forces and displacements of atoms along the MD trajectory at a certain temperature. Usually 100–200 uncorrelated configurations were used for the calculation. The obtained force constants were used to calculate the phonon dispersion and to solve the PBTE.

The LTC was determined by the self-consistent solution of the PBTE [1]. The dependence on the density of the reciprocal space grid and the cutoff radius of the effective force constants (EFCs) was thoroughly investigated. As a result, the following parameters were used: a grid of 12^3, the cutoff radii of the second- and third-order EFCs $R_{c2} = 6.2$ Å and $R_{c3} = 5.5$ Å, respectively. Note the large cutoff radius, especially for the third-order constants. This may be due to the resonant nature of the bonds in $CoSb_3$ [5]: the decay of EFCs is slow and non-monotonic. The largest obtained cutoff radius $R_c = 6.2$ Å was used in MTPs as the maximal radius for each partial atomic environment [19] in order to correctly reproduce the direct interaction between atoms.

Figure 1 shows the phonon dispersion curves and the cumulative dependence of the LTC on the phonon frequency for 300 K (an AIMD trajectory was used). The dispersion law is in good agreement with the previous calculations [5,41,45] and experiments [38–41]. The cumulative LTC shows fast increase for the phonons below 2 THz. The resolution of such phonons requires dense grids of k points or large system sizes. Therefore the systems with 12^3 unit cells were used for the Green-Kubo method, which made it possible to almost completely take into account all the necessary phonon modes.

C. Calculations via the Green-Kubo method

Finally, the MTPs were used in the calculation of LTC by the Green-Kubo method (equilibrium MD). The system size was chosen to be of $12 \times 12 \times 12$ unit cells (27 648 atoms), according to the results of solving the PBTE (Sec. II B). This size of the system is sufficient to describe the long-wavelength phonons involved in thermal transport. The simulation time step was 1 fs. The heat flux autocorrelation function (HFACF) was averaged over an ensemble of 20 independent systems.

All the results were examined for the convergence with respect to time step and simulation time. Each system was first equilibrated for 50 ps in the *NVT* ensemble, and then the HFACF was calculated for 2 ns in the *NVE* ensemble. The step for HFACF calculation was 1 fs, for a better description of its time dependence. The maximum correlation time was chosen to be 250, 200, and 150 ps, for 300, 500 and 700 K, respectively.

The thermal conductivity was calculated by the direct integration of the averaged HFACF. Figure 2 shows the average autocorrelator and the corresponding LTC for 500 K (the results for other temperatures are given in the Supplemental Material [46], Figs. 3 and 4. Note the strong oscillations of the HFACF and corresponding LTC. It is believed that such oscillations are the feature of complex systems with a large number of atoms in the unit cell [4,8,9]. Nevertheless, the average value of thermal conductivity became constant at $t \sim 100$ ps. The resulting value of LTC was determined by averaging over the last 50 ps.

III. MACHINE LEARNING INTERATOMIC POTENTIALS

A. Active learning

MTPs were trained to reproduce energies, forces, and stresses, obtained by DFT. Here "training" is optimization of the parameters of the model by minimization of the loss functional. Errors in energies and its first derivatives (forces and stresses) are simultaneously minimized with certain weights. We choose corresponding relative weights to be 1 for energy, 0.1 for forces, and 0.1 for stresses, in order to simultaneously increase the reliability and accuracy of the potential (see Ref. [47] for more details).

Three potentials with the same functional form but different values of parameters were trained for the three temperatures. The corresponding cells used for the training data contained 128 atoms. The cut-off radius of the potential was chosen to be 6.2 Å (see Sec. II B). The active learning scheme adapted from [19] was used to optimize the training process. The scheme is presented in Fig. 3. Briefly, the main steps are as follows:

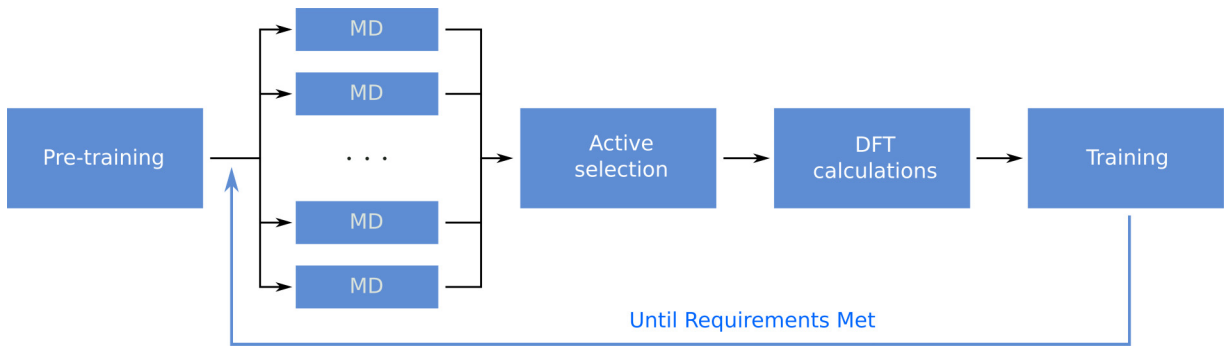

FIG. 3. The active learning scheme. The potentials are trained in a loop by automatically selecting the most representative configurations from independent MD runs until all of these runs stop producing extrapolative trajectories.

(1) The potential is pretrained on a short AIMD trajectory, of about 100 time steps. This can be considered as an initial approximation of the model.

(2) Classical equilibrium MD is performed at a certain temperature on an ensemble of independent systems. During each simulation, an active selection of atomic configurations is carried out.

(3) Active selection is repeated on all the configurations selected at the previous step. This is necessary because the systems in step (2) were independent, and therefore many of the selected configurations appear to be correlated.

(4) The configurations from the third step are calculated by DFT, with the same parameters as in AIMD. As a result, an "active" training set is formed.

(5) The potential is trained on the active training set.

(6) Steps (2)–(5) are repeated until no configurations were selected in any of the MD runs on step (2).

For active selection the algorithm described in [18,19] was used. In essence, it defines configurations on which the model extrapolates. The parameter which controls this process is the extrapolation grade. If the grade of configuration is above the threshold (large extrapolation), it is included in the training set. If the configuration correlates with those already present in the training set, it is skipped. The process can be viewed as the effective sampling of the phase space available to the system.

Active selection does not only increase the ability of the model to extrapolate. It also minimizes the number of configurations in the training set by sorting out most representative ones. This reduces the number of time-consuming quantum-mechanical calculations.

The condition for the stopping of the active-learning loop requires a separate discussion. The presented process of active learning aims to make the potential more reliable, that is, to avoid extrapolation during prediction of energies and forces. Thus, the accuracy criterion is not suitable. Since the potential should be used for the Green-Kubo method, the following condition was chosen: all the systems in step (2) evolve without exceeding the threshold up to 1 ns. As will be seen in what follows, this requirement is reasonable.

The described scheme has another advantage. Unless the temperature gradients are too large, the process of heat transfer is close to equilibrium. This is usually the case in practice. Therefore, the phase space occupied by the system is close to equilibrium one at an average temperature. Therefore the training on the equilibrium configurations is expected be sufficient for the LTC study.

TABLE I. Average errors for potential for each temperature $\Delta e = |E^{\mathrm{MTP}} - E^{\mathrm{DFT}}|/N_{at}$: the energy per atom; $|\Delta F| = |\mathbf{F}^{\mathrm{MTP}} - \mathbf{F}^{\mathrm{DFT}}|$: the absolute value of the force on atom; $\Delta\sigma = \sigma^{\mathrm{MTP}} - \sigma^{\mathrm{DFT}}$: the diagonal stress component; N_{conf}: the number of configurations in the active training set.

T, K	Δe (meV/at.)	$\lvert\Delta F\rvert$ (meV/Å)	$\Delta\sigma$ (GPa)	N_{conf}
300	0.08	20.0	0.29	271
500	0.13	34.0	0.29	717
700	2.56	53.2	0.25	652

B. Validation of the potentials

The validation of the obtained machine learning potentials was performed; 250 randomly selected configurations (not in the training set) were used. Table I presents the average errors in energies, forces, and stresses, and the number of configurations in the active training set for each potential. The average errors are rather low, and are of the order of typical errors of AIMD. Note that it was achieved with less than a thousand configurations in the training set.

Accurate reproducibility of forces is crucial for LTC calculation. The forces are directly used to obtain EFCs, thus all the phonon scattering properties for the PBTE. The forces acting on atoms due to local environment are also used to calculate heat flux [48]. Figure 4 shows the distribution of the error in force, depending on the force magnitude (for the validation set). The amplitude of thermal vibrations increases with temperature, which leads to the increase of forces acting on atoms. This in turn gives rise to the interpolation error of the machine learning potential. Hovewer, most of the errors remain close to the average value. In other words, relatively large errors are rare. Therefore we expect only small bias in the LTC.

Next we investigate the accuracy with which obtained interatomic potentials reproduce lattice dynamics. Figure 5 shows the density of phonon states and the dispersion law

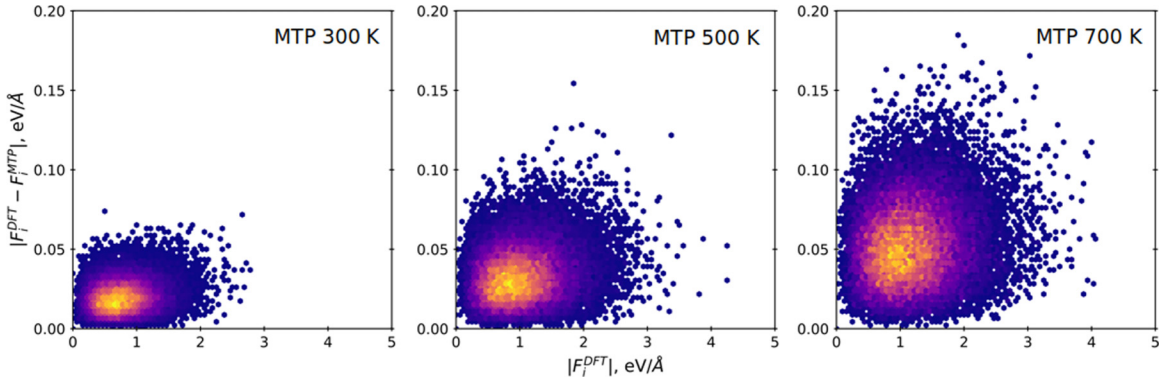

FIG. 4. The dependence of the error in force on the force magnitude. Left to right: 300 K, 500 K, 700 K. The color indicates the distribution of the error. Each distribution is normalized independently.

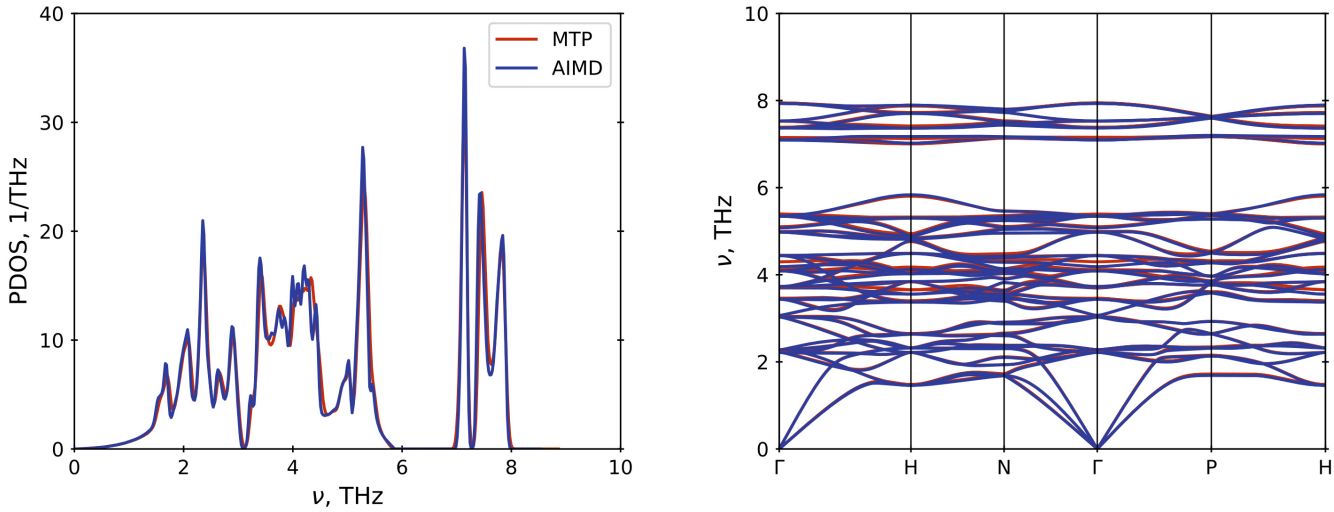

FIG. 5. Left: the density of phonon states, calculated with the effective force constants at 500 K. The force constants are obtained both for the classical trajectory with the MTP potential and for the AIMD trajectory. Right: corresponding phonon dispersion law.

calculated from the effective second-order force constants at 500 K. Two independent trajectories were used to obtain the result: the classical one obtained with MTPs and the one from AIMD. One can see the phonon dispersions are very close. For 300 and 700 K the results are similar (see Figs. 1 and 2 of the Supplemental Material [46]). A small difference exists in the optical part of the spectrum, but it almost does not contribute to thermal conductivity, as follows from Fig. 1.

Thus, phonons are accurately reproduced by the MTPs. A more rigorous method of validation is the thermal conductivity calculation, since it is caused by phonon scattering. The reproducibility of thermal conductivity is not straightforward, since the potentials were trained only on energy and its first derivatives. In addition, not every functional form (representation) of the potential allows one to reproduce the thermal conductivity [49]. These issues will be discussed further.

IV. RESULTS AND DISCUSSION

Figure 6 shows the results of the LTC calculations. We will discuss them in order. The results of PBTE with EFC obtained from the AIMD trajectories are shown by green circles. They are in good agreement with the experimental data. Similar results for the classical trajectories, generated with the MTP potentials, are presented by blue squares. They are close both to the AIMD results and the experiment. This means that the achieved accuracy of the reproduction of forces and energies is sufficient to describe phonon scattering.

Machine learning potentials have a flexible functional form and there may be many sets of parameters that lead to similar accuracy in the energy, forces, and stresses. It is not obvious that such different sets will lead to similar LTCs. In order to clarify this issue, four more potentials at 300 K were independently trained, according to the scheme described in Sec. III A. The validation was performed on the same 400 random configurations from the AIMD trajectory. Thermal conductivity was calculated using the Boltzmann equation and independent trajectories. The results are shown in Table II. As one can see, the potentials give similar errors in energy, forces, and stresses. The values of LTC also turned out to be close to each other. Thus, the statistical error in the calculation of thermal conductivity by solving the PBTE in Fig. 6 is of about the symbol size.

Finally, the results of the Green-Kubo method are represented by blue triangles. Despite the complexity of the system, the values are in good agreement with the results of solving the Boltzmann equation. One may notice that the GK method systematically gives a lower LTC value. This was expected, since the equilibrium dynamics is purely classical. The phonon occupation numbers and their relaxation times

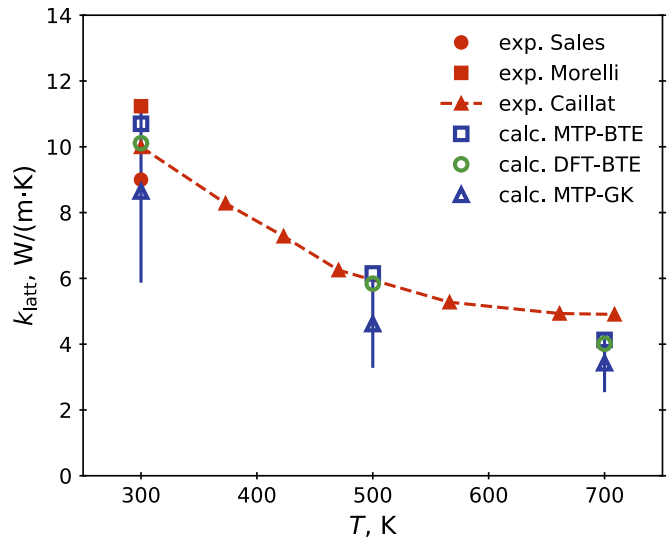

FIG. 6. The results of lattice thermal conductivity calculations (open symbols) and experimental data (filled symbols) [50–52]. DFT-BTE: solution of the PBTE with effective force constants from the AIMD trajectory; MTP-BTE: the same method, but trajectories with MTPs were used; MTP-GK: results of the Green-Kubo method for MTPs. Vertical lines: doubled standard deviation of the results of GK. The errors for the PBTE results are of the order of the symbols size.

TABLE II. Average validation errors for the potentials trained on four independently generated training sets at 300 K. The notations as in Table I.

	Δe (meV/at.)	$\lvert\Delta F\rvert$ (meV/Å)	$\Delta\sigma$ (GPa)	N_{conf}	κ_{BTE} [W/(m K)]
MTP-1	0.10	25.6	0.32	838	10.12
MTP-2	0.11	25.7	0.27	778	10.22
MTP-3	0.14	24.3	0.27	897	10.25
MTP-4	0.22	29.5	0.23	579	10.20

correspond to the classical limit, which lowers the LTC [8]. The deviation from the quantum PBTE result decreases with increasing temperature. In addition, the GK method takes into account all the orders of phonon scattering processes. This can also reduce thermal conductivity. We thus conclude that the results of different approaches agree with each other.

V. CONCLUSIONS

In conclusion, we have developed a method for automatic calculation of LTC for complex compounds by using machine learning potentials. Multicomponent potentials in the form of MTP were trained on the DFT data for the $CoSb_3$ skutterudite. Active learning was used to increase the reliability of the potential and reduce the number of time-consuming DFT calculations. Only a few hundred configurations are enough to build a sufficiently reliable potential that accurately reproduces harmonic and anharmonic parts of lattice dynamics. MTPs provide more than four orders of magnitude increase in computational speed: one time step on 64 cores for 128 atoms takes approximately 200 s for AIMD and 0.0025 s for MTP in our simulations. Furthermore, the methods based on classical MD, such as the Green-Kubo method, can be efficiently parallelized.

The potentials were used to calculate the LTC in two ways: using the PBTE and by the GK method. The results are in good agreement with each other and with the experiment. They also agree with the results of solving the PBTE for the AIMD trajectories. Thus, obtained machine learning potentials describe phonons and their scattering with high accuracy, although the training was performed on energy and its first derivatives (forces and stresses).

Active learning allows one to go beyond the spatial and temporal limits of AIMD, despite the MTPs were trained on relatively small systems. This is impressive, since training on a small system implies good reproduction of forces, stresses, and total energy only for similar systems. Generally speaking, a large system at a finite temperature is not a periodic repetition of a small system.

We also note that the systems of 128 atoms were used for the training. This means that the method can easily be extended to filled/compensated skutterudites or other similar systems. Such extension will be the aim of our future work. We believe that this approach, which does not require any experimental data, will be useful in the development of novel materials with complex crystal structures.

The input and output files for this work are available for download in the Mendeley Database [53].

ACKNOWLEDGMENTS

This work was supported by the Russian Science Foundation (Grant No. 18-13-00479).

[1] D. A. Broido, M. Malorny, G. Birner, N. Mingo, and D. A. Stewart, Appl. Phys. Lett. **91**, 231922 (2007).
[2] A. Ward, D. A. Broido, D. A. Stewart, and G. Deinzer, Phys. Rev. B **80**, 125203 (2009).
[3] A. Togo, L. Chaput, and I. Tanaka, Phys. Rev. B **91**, 094306 (2015).
[4] A. J. H. McGaughey and M. Kaviany, in *Advances in Heat Transfer*, edited by G. A. Greene, J. P. Hartnett, A. Bar-Cohen, and Y. I. Cho (Elsevier, New York, 2006), Vol. 39, pp. 169–255.
[5] R. Guo, X. Wang, and B. Huang, Sci. Rep. **5**, 7806 (2015).
[6] A. H. Romero, E. K. U. Gross, M. J. Verstraete, and O. Hellman, Phys. Rev. B **91**, 214310 (2015).
[7] T. Feng and X. Ruan, Phys. Rev. B **93**, 045202 (2016).
[8] Y. He, I. Savić, D. Donadio, and G. Galli, Phys. Chem. Chem. Phys. **14**, 16209 (2012).
[9] P. C. Howell, J. Chem. Phys. **137**, 224111 (2012).
[10] B. Fultz, Prog. Mater. Sci. **55**, 247 (2010).
[11] P. Korotaev, M. Belov, and A. Yanilkin, Comput. Mater. Sci. **150**, 47 (2018).
[12] J. Behler, J. Chem. Phys. **145**, 170901 (2016).
[13] A. V. Shapeev, *Computational Materials Discovery* (Royal Society of Chemistry, London, 2018), pp. 66–86.
[14] A. P. Bartók, J. Kermode, N. Bernstein, and G. Csányi, Phys. Rev. X **8**, 041048 (2018).
[15] X. Qian and R. Yang, Phys. Rev. B **98**, 224108 (2018).
[16] H. Babaei, R. Guo, A. Hashemi, and S. Lee, Phys. Rev. Mater. **3**, 074603 (2019).
[17] B. Cheng, E. A. Engel, J. Behler, C. Dellago, and M. Ceriotti, Proc. Natl. Acad. Sci. USA **116**, 1110 (2019).
[18] E. V. Podryabinkin and A. V. Shapeev, Comput. Mater. Sci. **140**, 171 (2017).
[19] K. Gubaev, E. V. Podryabinkin, G. L. W. Hart, and A. V. Shapeev, Comput. Mater. Sci. **156**, 148 (2019).
[20] N. Artrith and J. Behler, Phys. Rev. B **85**, 045439 (2012).
[21] L. Zhang, D.-Y. Lin, H. Wang, R. Car, and W. E, Phys. Rev. Mater. **3**, 023804 (2019).
[22] J. S. Smith, B. Nebgen, N. Lubbers, O. Isayev, and A. E. Roitberg, J. Chem. Phys. **148**, 241733 (2018).
[23] R. Jinnouchi, J. Lahnsteiner, F. Karsai, G. Kresse, and M. Bokdam, Phys. Rev. Lett. **122**, 225701 (2019).
[24] N. Bernstein, G. Csányi, and V. L. Deringer, npj Comput. Mater. **5**, 99 (2019).
[25] A. Shapeev, Multiscale Model. Simul. **14**, 1153 (2016).
[26] *Thermoelectrics Handbook: From Macro to Nano*, edited by D. Rowe (CRC Press, Taylor & Francis, FL, Boca Raton, 2006).

[27] *Modules, Systems, and Applications in Thermoelectrics*, edited by D. Rowe (CRC Press/Taylor & Francis, Boca Raton, FL, 2012).
[28] X. Shi, J. Yang, J. R. Salvador, M. Chi, J. Y. Cho, H. Wang, S. Bai, J. Yang, W. Zhang, and L. Chen, J. Am. Chem. Soc. **133**, 7837 (2011).
[29] A. Grytsiv, P. Rogl, H. Michor, E. Bauer, and G. Giester, J. Electron. Mater. **42**, 2940 (2013).
[30] G. Rogl, A. Grytsiv, P. Rogl, N. Peranio, E. Bauer, M. Zehetbauer, and O. Eibl, Acta Mater. **63**, 30 (2014).
[31] W.-S. Liu, B.-P. Zhang, L.-D. Zhao, and J.-F. Li, Chem. Mater. **20**, 7526 (2008).
[32] X. Su, H. Li, G. Wang, H. Chi, X. Zhou, X. Tang, Q. Zhang, and C. Uher, Chem. Mater. **23**, 2948 (2011).
[33] P. Korotaev and A. Yanilkin, J. Mater. Chem. C **5**, 10185 (2017).
[34] G. Kresse and D. Joubert, Phys. Rev. B **59**, 1758 (1999).
[35] G. Kresse and J. Furthmüller, Phys. Rev. B **54**, 11169 (1996).
[36] J. P. Perdew, K. Burke, and M. Ernzerhof, Phys. Rev. Lett. **77**, 3865 (1996).
[37] R. Hanus, X. Guo, Y. Tang, G. Li, G. J. Snyder, and W. G. Zeier, Chem. Mater. **29**, 1156 (2017).
[38] H. D. Lutz and G. Kliche, Phys. Status Solidi B **112**, 549 (1982).
[39] G. S. Nolas, G. A. Slack, T. Caillat, and G. P. Meisner, J. Appl. Phys. **79**, 2622 (1996).
[40] G. S. Nolas and C. A. Kendziora, Phys. Rev. B **59**, 6189 (1999).
[41] M. Rotter, P. Rogl, A. Grytsiv, W. Wolf, M. Krisch, and A. Mirone, Phys. Rev. B **77**, 144301 (2008).
[42] LAMMPS Molecular Dynamics Simulator, http://lammps.sandia.gov/.
[43] O. Hellman, P. Steneteg, I. A. Abrikosov, and S. I. Simak, Phys. Rev. B **87**, 104111 (2013).
[44] O. Hellman and I. A. Abrikosov, Phys. Rev. B **88**, 144301 (2013).
[45] B. Huang and M. Kaviany, Acta Mater. **58**, 4516 (2010).
[46] See Supplemental Material at http://link.aps.org/supplemental/10.1103/PhysRevB.100.144308 for additional figures.
[47] I. I. Novoselov, A. V. Yanilkin, A. V. Shapeev, and E. V. Podryabinkin, Comput. Mater. Sci. **164**, 46 (2019).
[48] A. P. Thompson, S. J. Plimpton, and W. Mattson, J. Chem. Phys. **131**, 154107 (2009).
[49] A. Rohskopf, H. R. Seyf, K. Gordiz, T. Tadano, and A. Henry, npj Comput. Mater. **3**, 27 (2017).
[50] D. T. Morelli, T. Caillat, J.-P. Fleurial, A. Borshchevsky, J. Vandersande, B. Chen, and C. Uher, Phys. Rev. B **51**, 9622 (1995).
[51] T. Caillat, A. Borshchevsky, and J. Fleurial, J. Appl. Phys. **80**, 4442 (1996).
[52] B. C. Sales, D. Mandrus, B. C. Chakoumakos, V. Keppens, and J. R. Thompson, Phys. Rev. B **56**, 15081 (1997).
[53] P. Korotaev, I. Novoselov, A. Yanilkin, and A. Shapeev, Data cite for "Accessing thermal conductivity of complex compounds by machine learning interatomic potentials", http://dx.doi.org/10.17632/t6hz579sry.1 (2019).